ACS Catalysis

pubs.acs.org/acscatalysis

Research Article

Supported Molybdenum Carbide Nanoparticles as an Excellent Catalyst for CO_2 Hydrogenation

Marc Figueras, Ramón A. Gutiérrez, Francesc Viñes, Pedro J. Ramírez, José A. Rodriguez,* and Francesc Illas*

Cite This: *ACS Catal.* 2021, 11, 9679−9687

Read Online

ACCESS | Metrics & More | Article Recommendations | Supporting Information

ABSTRACT: Experiments under controlled conditions show that MoC_x nanoclusters supported on an inert Au(111) support are efficient catalysts for CO_2 conversion, although with a prominent role of stoichiometry. In particular, C-deficient nanoparticles directly dissociate CO_2 and rapidly become deactivated. On the contrary, nearly stoichiometric nanoparticles reversibly adsorb/desorb CO_2 and, after exposure to hydrogen, CO_2 converts predominantly to CO with a significant amount of methanol and no methane or other alkanes as reaction products. The apparent activation energy for this process (14 kcal/mol) is smaller than that corresponding to bulk δ-MoC (17 kcal/mol) or a Cu(111) benchmark system (25 kcal/mol). This trend reflects the superior ability of $MoC_{1.1}$/Au(111) to bind and dissociate CO_2. Model calculations carried out in the framework of density functional theory provide insights into the underlying mechanism suggesting that CO_2 hydrogenation on the hydrogen-covered stoichiometric MoC_x nanoparticles supported on Au(111) proceeds mostly under an Eley−Rideal mechanism. The influence of the Au(111) is also analyzed and proven to have a role on the final reaction energy but almost no effect on the activation energy and transition state structure of the analyzed reaction pathways.

KEYWORDS: *CO_2 hydrogenation, MoC_x nanoparticles, XPS, TPD, DFT*

INTRODUCTION

Since the 1970s, transition-metal carbides have been suggested as an alternative to catalysts based on expensive late transition metals for a wide variety of hydrogenation reactions.[1−4] In many new catalysts, metal carbides nanoparticles (NPs) are dispersed on oxides and zeolites[5,6] but little is known about the specific phenomena which determine the hydrogenation capabilities of these systems. In principle, size effects and the carbon/metal ratio could affect the behavior of a NP.[2,7,8] Experimental studies for H_2 adsorption on NPs of $MoC_{0.6}$ and $MoC_{1.1}$ supported on Au(111), complemented by computational modeling, have shown that these systems are extremely efficient for the cleavage of the H−H bond at room temperature and the storage of H adatoms.[9] For H_2/$MoC_{1.1}$/Au(111), the results of temperature-programmed desorption (TPD) showed H_2 evolution between 350 and 450 K and a H/C ratio close to two, a value much larger than the one observed on bulk rock-salt δ-MoC surfaces, thus pointing out that $MoC_{1.1}$ NPs can act as H sponges, where H_2 can be easily adsorbed or desorbed, posing them as hot hydrogen reservoirs for catalytic applications.[9]

In this study, we examine the performance of MoC_x/Au(111) surfaces in the catalytic hydrogenation of carbon dioxide. This chemical transformation was chosen as a test due to its relevance for the control of air pollution and the production of high value chemicals in C_1 catalysis.[10,11] It is nowadays well-accepted that many activities involving the burning of fossil fuels in our industrial society have led to an excessive concentration of CO_2 in the atmosphere and major environmental problems.[10] In order to mitigate these harmful effects, CO_2 capture, storage, and, specially, its conversion to valuable chemicals or commodity goods have become an urgent need.[11,12]

Previous research has shown that metal carbides can hydrogenate CO_2 to give CO, oxygenates, and alkanes.[13,14] This diversity of products comes as a result of the effects of the carbon/metal ratio on the reactivity of a carbide toward CO_2. For example, on an orthorhombic β-Mo_2C(001) surface, the CO_2 molecule is strongly adsorbed, the first C−O breaks below 200 K, and the second around room temperature.[2] A more detailed study showed that the effect of the surface termination is also important. In fact, density functional theory (DFT) calculations predicted, and experiments confirmed, that the orthorhombic β-Mo_2C(001) Mo-terminated polar surface leads to a spontaneous cleavage of a C−O bond in CO_2 and

Received: April 16, 2021
Revised: July 7, 2021
Published: July 18, 2021

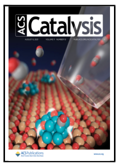

the carbon monoxide formation.[15] The same study showed that on a β-$Mo_2C(001)$ C-terminated polar surface or on a δ-MoC(001) nonpolar surface, the CO_2 molecule is activated, yet the C−O bond prevails. These results illustrate the huge impact the carbon/metal ratio has on the chemical and catalytic properties of molybdenum carbides and explains why the hydrogenation of CO_2 on β-Mo_2C powders produces a large amount of CO, methane, and light alkanes.[13,16] On the other hand, bulk δ-MoC exhibits a promising behavior for the conversion of CO_2 into methanol.[14] On carbides with a carbon/metal ratio close to one such as ZrC, TaC, NbC, HfC, TiC, or δ-MoC, the CO_2 molecule does not undergo spontaneous dissociation.[14,15,17] It adsorbs on C sites of the carbide surface with the formation of $C{=}CO_2$ bonds and its dissociation is assisted by hydrogen adatoms.[14]

The large amounts of H that can be accumulated in the MoC_x/Au(111) systems[8] may give the carbide NPs special properties for the catalytic conversion of CO_2, arising from the diversity of easily interconvertible surface hydrogen species and the catalytic smoothness achieved by H-coverage effects.[9] In this work, we use a combination of catalytic testing, X-ray photoelectron spectroscopy (XPS) measurements, and calculations based on DFT to investigate the hydrogenation of CO_2 on carbon-poor ($MoC_{0.6}$) and carbon-rich ($MoC_{1.1}$) NPs supported on Au(111) and present evidence that the latter constitute efficient catalysts for CO_2 decomposition to CO and methanol with a large selectivity to the former. The theoretical study consistently shows that the effect of preadsorbed H is crucial. The calculations evidence a systematic qualitative trend, preadsorbed H leads to a decrease in the energy barriers involved in the CO_2 hydrogenation steps, and even triggers an Eley−Rideal mechanism for the H-assisted CO_2 dissociation.

EXPERIMENTAL PROCEDURE

The catalytic performance of the carbon-poor ($MoC_{0.6}$) and carbon-rich ($MoC_{1.1}$) NPs supported on Au(111) was investigated in an instrument which combined a batch reactor with an ultrahigh-vacuum (UHV) chamber for surface characterization with XPS, TPD, and ion-scattering spectroscopy. The sample could be moved between the UHV chamber and the microreactor without exposure to air.

The MoC_x/Au(111) systems were prepared following a methodology described in previous works, where the interaction of these systems with methane and molecular hydrogen was examined.[8,9,18] In short, the NPs were synthesized by deposition of the Mo metal onto a reactive multilayer of ethylene (C_2H_4), which was resting physisorbed on a Au(111) substrate at low temperatures (90−100 K).[18] Upon heating to 750 K, the unreacted C_2H_4 desorbed and the MoC_x NPs were left on the gold substrate. The Mo → MoC_x transformations could be followed using a combination of XPS, TPD, and scanning tunneling microscopy (STM).[18] In this synthetic approach, one can control the C/Mo ratio in the NPs from 0.6 (C-poor) to 1.1 (C-rich).[8,9] XPS was used to determine this ratio and we utilized as reference previous values measured in our instrument for the C 1s and Mo 3d regions of bulk MoC and Mo_2C.[14] For the bulk sample of MoC, our XPS measurements pointed to a C/Mo ratio of 0.98−0.96 in good agreement with the ratio typically observed for bulk samples of one-to-one carbides.[19−21] Images acquired using STM have shown that the generated NPs by this synthetic procedure are relatively small (0.8−1.5 nm) and grew over the face-centered cubic (fcc) troughs located on either side of the elbows of the reconstructed Au(111) support.[18] Previous works have examined the reactivity of these MoC_x/Au(111) surfaces toward cyclohexene,[22] methane,[8] and H_2.[9]

The catalytic activity for CO_2 hydrogenation of the MoC_x/Au(111) systems was examined at temperatures in the range of 500−600 K. After characterization in the UHV chamber, the sample was transferred to the batch reactor at room temperature, the reactant gases were introduced [0.049 MPa (0.5 atm) of CO_2 plus 0.441 MPa (4.5 atm) of H_2], and finally, the catalyst was rapidly heated to the reaction temperature. The evolution of the gas composition inside the reactor was followed using a gas chromatograph with a flame ionization detector,[14] collecting data (CH_3OH, CH_4, and CO production) at intervals of 10 to 15 min for up to 16 h. The yields of carbon monoxide, methane, and methanol in the catalytic tests were normalized by the active area exposed by the sample and the total reaction time. The kinetic experiments to obtain the data for the Arrhenius plots were performed in the limit of low conversion (<5%).

MATERIALS, MODELS, AND COMPUTATIONAL DETAILS

The direct and hydrogen-assisted CO_2 dissociation on MoC_x/Au has been studied using a series of suitable models and DFT calculations. The models start from $Mo_{12}C_{12}$ NPs supported on a $p(6 \times 6)$ supercell of Au(111) following the approach described in a previous work investigating the hydrogen storage capability of these systems.[9] In view of the huge amount of possible adsorption sites, several pathways were first considered for the CO_2 direct dissociation on the $Mo_{12}C_{12}$/Au(111) model, and then, a set of these pathways were explored on the same $Mo_{12}C_{12}$ NPs but removing the Au(111) support, that is, ignoring the direct support effect. Results entail a clear resemblance between gas and supported models, and, in consequence, the effect of hydrogen coverage on the reaction profile was studied on the gas-phase models. This strategy is based on the observed ability of carbide NPs to store hydrogen[9] and allows one to tackle a vast number of reaction pathways under different hydrogen coverage at a reasonable computational cost. For the MoC_x/Au(111) systems, the main modifier of the surface chemistry on the carbide NPs should be hydrogen and not the inert gold substrate.[9]

The corresponding models are referred to as $Mo_{12}C_{12}$-sup (supported) and $Mo_{12}C_{12}$-free (in vacuum). In addition, for the $Mo_{12}C_{12}$-free model, we considered three different situations where the CO_2 to CO + O elementary step is explored. In the first one, the atomic structure of the $Mo_{12}C_{12}$ NPs is frozen as in the $Mo_{12}C_{12}$-sup and will be denoted as $Mo_{12}C_{12}$-free-1; in the second one, the position of the atoms that would be in contact with the Au surface is frozen as in $Mo_{12}C_{12}$-sup and the rest are allowed to relax ($Mo_{12}C_{12}$-free-2) and, finally, all atoms in the $Mo_{12}C_{12}$-free NP are free to relax ($Mo_{12}C_{12}$-free). The initial atomic structure of the NP model was obtained by mimicking largely stable gas-phase TiC NPs as previously reported.[23] These TiC NP models were acquired through interatomic potentials and the resulting atomic structure used as input for geometry optimization by means of DFT calculations. For the 21 low-energy structures of $Ti_{12}C_{12}$ reported by Lamiel-Garcia *et al.*,[23] Ti atoms were substituted by Mo atoms and the resulting structure was fully reoptimized by DFT calculations using the approaches described below. Resulting models are undoubtedly similar to their TiC counterparts, an expected outcome as both TiC and the δ-MoC polymorph exhibit the same rock-salt structure. For additional information regarding the structure of this type of NPs, we refer the reader to recent work describing a rather large set and their interaction with ethylene.[24]

All energy values reported in this work were obtained through periodic DFT calculations using large enough supercells so that the interaction between the supported NPs in periodically repeated images is negligible. The supercell size and **k**-point grid used depend on whether the Au(111) support is included or not. Thus, for the explicitly supported $Mo_{12}C_{12}$ NPs models, a 3×3×1 Monkhorst−Pack grid of special **k**-points was used, while calculations involving unsupported NPs were carried out at the $\boldsymbol{\Gamma}$ point only. The Au(111) support was represented using slab models including four atomic layers with the two upmost layers allowed to relax and the two bottommost ones kept frozen so as to provide a bulk environment to the surface region. This type of modeling metal surfaces is a rather standard approach employed by many authors; see, for instance, the kinetic Monte Carlo study of CO_2 hydrogenation on Ni(111),[25] the electroreduction of CO by Cu surfaces,[26] and references therein. Further details can be found in two very recent reviews.[27,28]

All calculations were carried out using the Vienna *Ab initio* Simulation Package (VASP) code,[29] employing the Perdew−Burke−Ernzerhof (PBE) exchange−correlation functional,[30] which has been determined as a suitable functional to describe Mo-based carbides.[31] Moreover, dispersion terms have been accounted by the Grimme D3 correction.[32] The Kohn−Sham equations were solved within a plane-wave basis set with a cutoff of 415 eV, while the effect of core electrons into the valence electron density was included through the projected augmented wave method as implemented by Kresse and Joubert.[33] Spin polarization has been found to be negligible on supported cases but accounted for in the gas-phase models as there it might have a significant effect. Convergence thresholds for the total energy and atomic forces were set to 10^{-5} eV and 0.01 eV Å^{-1}, respectively. Finally, transition state (TS) structures have been located by means of the climbing-image nudged-elastic-band (CI-NEB) method[34] and characterized by frequency analysis through the diagonalization of the corresponding block of the Hessian matrix with elements computed with finite differences of 0.03 Å of analytic gradients.

■ RESULTS AND DISCUSSION

Adsorption of CO_2 on MoC_x/Au(111) Surfaces: XPS Studies. In a first set of experiments, we investigated the adsorption of carbon dioxide on C-poor, $MoC_{0.6}$/Au(111), and C-rich, $MoC_{1.1}$/Au(111), NPs of molybdenum carbide dispersed on a gold substrate. Figure 1 displays C and O 1s XPS spectra collected after dosing CO_2 at 300 K. The Au(111) substrate does not adsorb the CO_2 molecule. A drastic change in reactivity is seen after the deposition of $MoC_{0.6}$ NPs. In the C 1s and O 1s regions, features are detected that denote the presence of C, O, and CO species on the surface.[35] These features indicate that the carbon dioxide undergoes partial ($CO_2 \rightarrow CO + O$) and complete ($CO_2 \rightarrow C + 2O$) decomposition on the $MoC_{0.6}$/Au(111) surface. In this system, the behavior is very similar to that found for CO_2 adsorbed on a bulk β-Mo_2C(001) surface where the C/Mo ratio is 0.5.[35]

$MoC_{1.1}$/Au(111) exhibited a reactivity toward CO_2 which was very different from that found on $MoC_{0.6}$/Au(111). In $MoC_{1.1}$/Au(111), the XPS data in Figure 1 indicate that CO_2 was adsorbed molecularly at 300 K and desorbed intact upon heating to 450 K. After increasing the C/Mo ratio to 1.1, the carbide still binds CO_2 well, but it does not dissociate the C−O bonds of the molecule. It has a behavior very similar to that observed for bulk δ-MoC,[14] but in $MoC_{1.1}$/Au(111), the adsorption bond of CO_2 is stronger. As we will see below, this difference facilitates the activation and conversion of CO_2 to methanol on the $MoC_{1.1}$/Au(111) surface upon reaction with hydrogen.

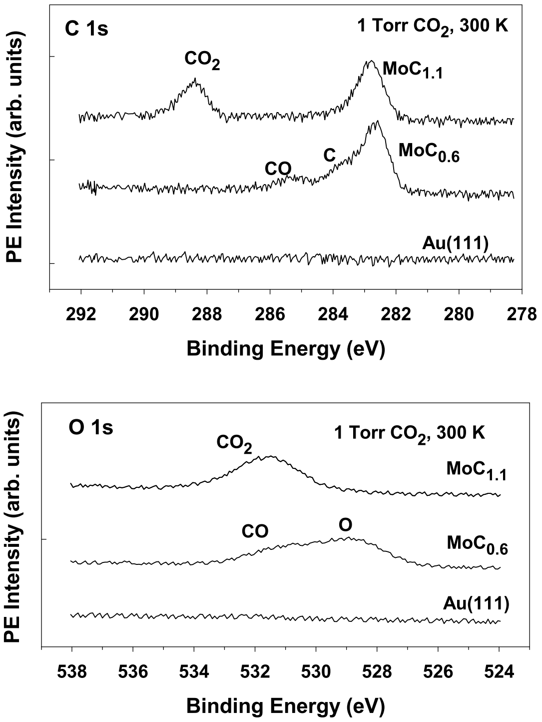

Figure 1. C 1s (top panel) and O 1s (bottom panel) XPS spectra recorded after exposing Au(111), $MoC_{0.6}$/Au(111), and $MoC_{1.1}$/Au(111) surfaces to 1 Torr of CO_2 at 300 K for 5 min in a microreactor. After exposure to CO_2, the gas was pumped out from the microreactor and the samples were transferred to a UHV chamber to collect the XPS spectra. In the surfaces with MoC_x NPs, the coverage of Mo was close to 0.3 monolayer (ML) in both cases.

Conversion of CO_2 to CO and CH_3OH on MoC_x/Au(111) Surfaces: Kinetic Studies. On a previous study, we have shown that MoC_x NPs are extremely active for the binding and dissociation of H_2.[9] The hydrogen on the MoC_x/Au(111) surfaces can be present as adatoms, molecules in a *Kubas* adsorption mode or form CH_x species that easily release hydrogen upon heating.[9] In principle, these systems are ideal for hydrogenation processes. Consequently, in the present study, we have investigated the hydrogenation of CO_2 on C-poor, $MoC_{0.6}$/Au(111), and C-rich, $MoC_{1.1}$/Au(111), systems. Both of them act as sponges for hydrogen adsorption/desorption.[9]

Figure 2 summarizes the results for the hydrogenation of CO_2 on $MoC_{0.6}$/Au(111). Initially, the main product of the reaction is methane, with CO as a secondary product, and a trace of methanol. This result can be explained using the CO_2 adsorption data reported in Figure 1 for the $MoC_{0.6}$/Au(111) system. The full dissociation of CO_2 produces C atoms that eventually are hydrogenated to yield methane. The pristine $MoC_{0.6}$/Au(111) surface is a very good catalyst for CO_2 methanation, but the accumulation of O adatoms, bottom

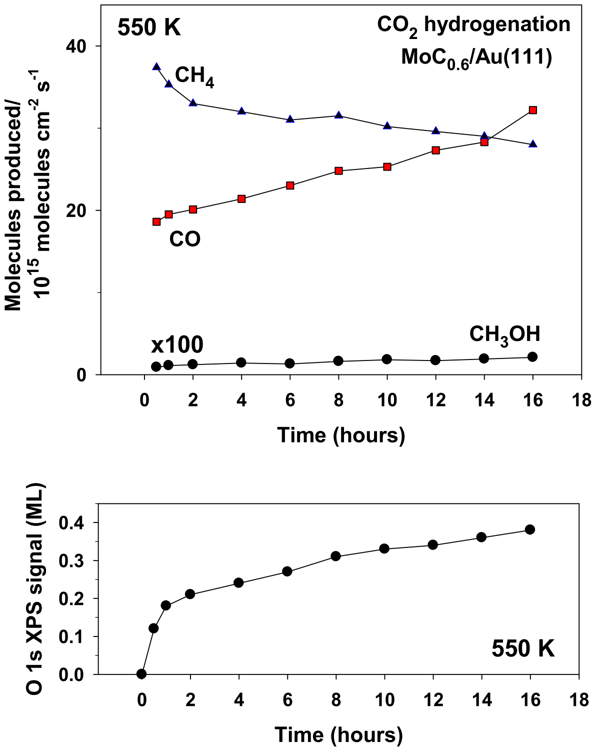

Figure 2. Top panel: Production of CH_4, CO, and CH_3OH during the hydrogenation of CO_2 on a Au(111) surface precovered with 0.3 ML of $MoC_{0.6}$. Bottom panel: Amount of oxygen measured with XPS after different CO_2 hydrogenation times on the $MoC_{0.6}$/Au(111) catalyst. T = 550 K, $P(CO_2)$ = 0.5 atm, and $P(H_2)$ = 4.5 atm.

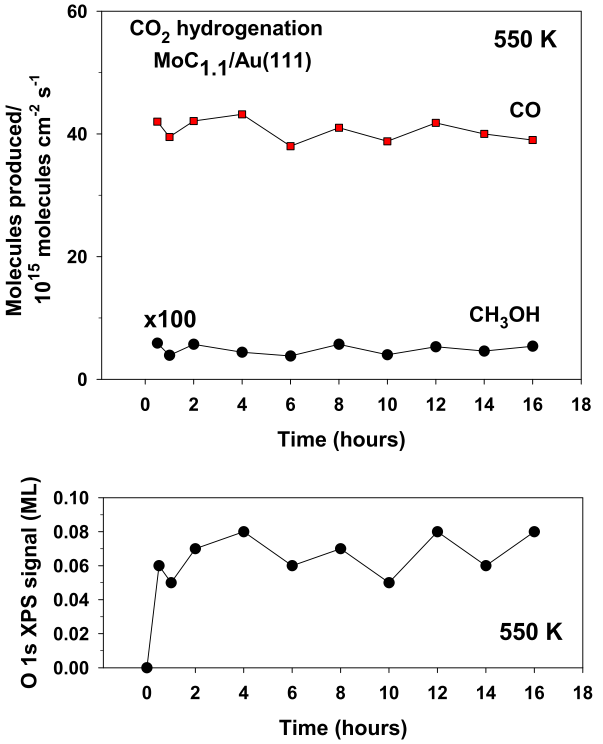

Figure 3. Top panel: Production of CH_4, CO, and CH_3OH during the hydrogenation of CO_2 on a Au(111) surface precovered with 0.3 ML of $MoC_{1.1}$. Bottom panel: Amount of oxygen measured with XPS after different CO_2 hydrogenation times on the $MoC_{1.1}$/Au(111) catalyst. T = 550 K, $P(CO_2)$ = 0.5 atm, and $P(H_2)$ = 4.5 atm.

panel in Figure 2, changes the selectivity of the catalyst and eventually CO becomes the main reaction product. The O adatoms probably block the highly active sites that fully decompose CO_2 on the $MoC_{0.6}$/Au(111) surface. Post-reaction characterization with XPS showed that O adatoms were always the dominant species on this surface with a very small amount (<0.05 ML) of a carbonate. The hydrogen atoms generated by H_2 dissociation on this system are not reactive enough to remove the O adatoms yielded by CO_2 decomposition, the catalyst is metastable, and the carbide NPs transform into a highly stable oxycarbide which also has been detected on surfaces and powders of bulk Mo_2C.[14,16,36,37] The product distribution seen for the hydrogenation of CO_2 on $MoC_{0.6}$/Au(111) is similar to that reported for NPs of Mo_2C which are mainly methanation or Fischer−Tropsch catalysts.[13]

On the other hand, Figure 3 summarizes the results for the hydrogenation of CO_2 on $MoC_{1.1}$/Au(111). Conversely, here, no production of methane was detected. The distribution of reaction products did not change with time, and the main product of the catalytic process was CO with a significant amount of methanol also being produced. As seen in Figure 1, the dissociation of CO_2 on $MoC_{1.1}$/Au(111) is negligible and the system cannot be a good methanation catalyst. The theoretical calculations described below indicate that the hydrogen present in $MoC_{1.1}$/Au(111)[9] facilitates the dissociation of CO_2 into CO by the reverse water−gas shift reaction. Post-reaction characterization with XPS showed that the amount of oxygen deposited on the $MoC_{1.1}$/Au(111) catalyst was very small, see the bottom panel in Figure 3, and most of the O atoms generated by the partial dissociation of CO_2 were rapidly hydrogenated to evolve as gaseous water. According to post-reaction XPS, the surface of the $MoC_{1.1}$/Au(111) catalyst was essentially clean ($\theta_O \sim 0.06$ ML) without carbonates or other C-containing molecules. A comparison of the results in Figures 2 and 3 indicates that the C/Mo ratio in the MoC_x NPs has a tremendous effect on the surface reactivity and the product distribution for CO_2 hydrogenation. The behavior seen for C-rich $MoC_{1.1}$/Au(111) is very different from that seen on C-poor $MoC_{0.6}$/Au(111) or for unsupported NPs of Mo_2C.[13] Thus, the C/Mo ratio can be a quite useful parameter to tune when dealing with CO_2 hydrogenation on carbide NPs.

Since the $MoC_{1.1}$/Au(111) catalyst is stable with time, see Figure 3, one was able to study, in a reproducible way, the hydrogenation of CO_2 at different temperatures. Figure 4 displays an Arrhenius plot for CO_2 hydrogenation to methanol on $MoC_{1.1}$/Au(111). The plain Au(111) substrate is not active for a $CO_2 \rightarrow CH_3OH$ conversion. For comparison, we also include in Figure 4 results for methanol synthesis on Cu(111), a common benchmark, and on bulk δ-MoC.[14] In addition, using the surface atomic density of Au(111) and assuming that all the Mo sites are active, we estimated that minimum TOFs of 0.41 CH_3OH produced molecules site^{-1} s^{-1} at 600 K and 0.07 CH_3OH produced molecules site^{-1} s^{-1} at 500 K. These TOF values are significantly bigger than those reported for Cu(111), Cu(110), polycrystalline Cu, and Cu/ZnO powder catalysts.[38,39] Clearly, $MoC_{1.1}$/Au(111) is a very good catalyst for methanol synthesis. This remarkable result highlights the importance of controlling the C/Mo ratio when dealing with MoC_x NPs as catalysts.

As can be seen in Figure 4, the apparent activation energy for methanol production is reduced from 25 kcal/mol on

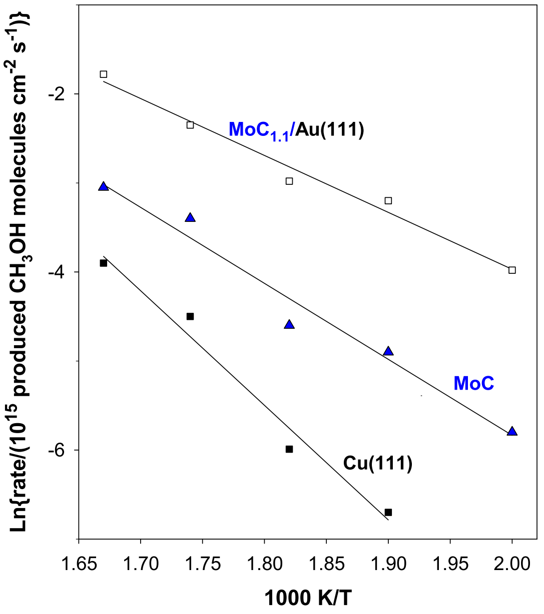

Figure 4. Arrhenius plots for CO_2 hydrogenation on Cu(111), bulk δ-MoC, and a Au(111) surface with 0.3 ML of $MoC_{1.1}$. $P(CO_2)$ = 0.5 atm and $P(H_2)$ = 4.5 atm.

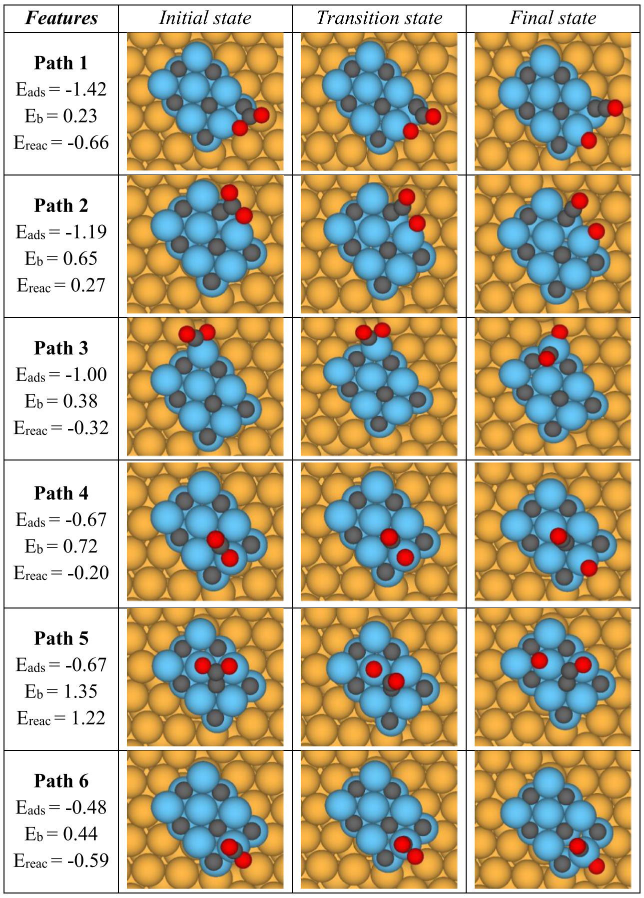

Figure 5. Main considered paths for CO_2 direct dissociation on $Mo_{12}C_{12}$/Au(111). Blue, black, red, and yellow spheres correspond to Mo, C, O, and Au atoms, respectively. Listed on the left side of the figure are calculated results for the adsorption energy (E_{ads}), energy barrier for CO_2 dissociation (E_b), and the reaction energy (E_{reac}). All energies are given in eV.

Cu(111) to 17 kcal/mol on bulk δ-MoC and 14 kcal/mol on the $MoC_{1.1}$/Au(111) surface. The atoms in the $MoC_{1.1}$ NPs are orders of magnitude more efficient for the $CO_2 \rightarrow CH_3OH$ hydrogenation than the atoms in the Cu(111) benchmark. Furthermore, the $MoC_{1.1}$/Au(111) system exposed a much lower concentration of carbide sites per surface area than bulk δ-MoC, but it had a much better catalytic performance. These trends probably reflect the superior ability of $MoC_{1.1}$/Au(111) to bind and dissociate H_2.[9]

Adsorption and Activation of CO_2 on C-rich MoC_x/Au(111) Surfaces: DFT Studies. The experimental results in Figures 1−4 indicate that C-rich ($MoC_{1.1}$) carbide NPs are the systems to focus when attempting a controlled and stable conversion of CO_2 into CO and methanol. In a first step, the adsorption mode and energy of CO_2 have been studied at various distinct sites of the $Mo_{12}C_{12}$ NP supported on Au(111)—the $Mo_{12}C_{12}$-sup model—which were compared to previous results for CO_2 adsorption on the extended δ-MoC(001) surface. For this extended surface, calculations with the PBE-D2 method predicted adsorption energy values ∼1.5 eV;[15] the use of a more accurate parametrization of the contribution dispersion by means of the PBE-D3 approach reduces these values to the 1.0−1.2 eV range depending on the site.[17] These values have been obtained by considering a minimum unit cell for the δ-MoC(001) slab model and, hence, with an atomic structure that closely resembles that of the ideal, bulk-cut, surface. However, recent work has shown that this surface exhibits a noticeable reconstruction and, hence, the adsorption energy with respect to the ideal surface is overestimated by ∼0.6 eV.[40] Consequently, a better estimate of the adsorption energy of CO_2 on the reconstructed δ-MoC(001) surface is 0.4−0.6 eV, again depending on the site. For the $Mo_{12}C_{12}$-sup model, the CO_2 adsorption energy ranges from 0.5 to 1.4 eV, the stronger adsorption corresponding to a quite unique site involving a highly undercoordinated C atom, see Figure 5. The concentration of this type of site is likely to be very small and probably biased using the used model. Nevertheless, discarding this special site still leaves several sites where the CO_2 adsorption energy is noticeably larger than for the extended surface, in agreement with experimental results.

Next, we consider a series of well-defined pathways for the CO_2 direct dissociation on $Mo_{12}C_{12}$-sup starting from each of the adsorption sites mentioned above and displayed in Figure 5. Excluding the rather infrequent sites involving a highly undercoordinated C atom and a very low coordinated Mo site, the direct CO_2 dissociation to CO and O involves rather large energy barriers, which is in agreement with experiments indicating that CO_2 does not directly dissociate on the C-rich $MoC_{1.1}$/Au(111) system. The quite low-energy barrier for the mentioned undercoordinated sites is interpreted here as a limitation of the present model as, even if eventually present in the experiment, the number of this type of sites will be very small and they are likely to be immediately passivated by C or O atoms produced by dissociation of CO_2.

To investigate the effect of the underlying Au(111) surface into the chemistry of the $Mo_{12}C_{12}$ NPs, we considered the different models where the structure of the NPs is as in the supported case but without the support and either frozen ($Mo_{12}C_{12}$-free-1), partially relaxed ($Mo_{12}C_{12}$-free-2), or totally relaxed ($Mo_{12}C_{12}$-free), as indicated above. Table 1 summarizes the results for these three types of unsupported particles which evidence small variations both in the adsorption energies and energy barriers. The reaction energies are somehow more

Table 1. Effect of the Au Substrate on the Energy Profile for Representative Pathways for CO_2 Dissociation[a]

energy barrier	path 2	path 3	path 5
$Mo_{12}C_{12}$-sup	0.65	0.38	1.35
$Mo_{12}C_{12}$-free-1	0.83	0.36	1.03
$Mo_{12}C_{12}$-free-2	0.97	0.35	1.19
$Mo_{12}C_{12}$-free	0.79	0.44	1.52
CO_2 adsorption energy	path 2	path 3	path 5
$Mo_{12}C_{12}$-sup	−1.19	−1.00	−0.68
$Mo_{12}C_{12}$-free-1	−1.82	−1.37	−1.03
$Mo_{12}C_{12}$-free-2	−1.38	−1.25	−0.72
$Mo_{12}C_{12}$-free	−1.21	−1.09	−0.41
CO*+O* adsorption energy	path 2	path 3	path 5
$Mo_{12}C_{12}$-sup	−0.92	−1.32	0.54
$Mo_{12}C_{12}$-free-1	−1.49	−1.57	−0.40
$Mo_{12}C_{12}$-free-2	−0.91	−1.48	−0.22
$Mo_{12}C_{12}$-free	−0.61	−1.25	0.25
reaction energy	path 2	path 3	path 5
$Mo_{12}C_{12}$-sup	0.27	−0.32	1.22
$Mo_{12}C_{12}$-free-1	0.33	−0.21	0.63
$Mo_{12}C_{12}$-free-2	0.47	−0.23	0.50
$Mo_{12}C_{12}$-free	0.60	−0.16	0.67

[a] The different models are described in the main text. All values are given in eV.

affected, but the analysis of the results shows that this can, in part, be explained from the fact that the supported NP is partly stabilized by the presence of the Au substrate. To estimate the influence of the NP structure on the reaction energy, we analyzed the structural difference in the $Mo_{12}C_{12}$ NP when reactants (CO_2) or products (CO + O) are adsorbed. To this end, we computed the energy of the $Mo_{12}C_{12}$ NP at each geometry once reactants and products have been removed from the fully optimized $Mo_{12}C_{12}$-free model. For the $Mo_{12}C_{12}$-sup structure, the underlying Au support has also been removed. For convenience, we use SupR and SupP to refer to the structure of the $Mo_{12}C_{12}$-sup NP that is obtained once the reactants, products, and substrate are removed from the optimized structure in the $Mo_{12}C_{12}$-sup model. Following the same logic, the corresponding notation for the $Mo_{12}C_{12}$-free model is FreeR and FreeP. With these definitions, the influence of the Au substrate in the reaction energy, Δ_{sup}, can be obtained as

$$\Delta_{sup} = \frac{(E_{SupP} - E_{SupR}) - (E_{FreeP} - E_{FreeR})}{E_{sup}^{Reac} - E_{free}^{Reac}} \quad (1)$$

where E_{sup}^{Reac} and E_{free}^{Reac} are the actual reaction energies in the supported model and free model that can be extracted from Table 1. From eq 1, it turns out that a Δ_{sup} value close to 1 implies that the differences in reaction energy between the $Mo_{12}C_{12}$-free and $Mo_{12}C_{12}$-sup models can be completely ascribed to the structural differences between the $Mo_{12}C_{12}$-free and $Mo_{12}C_{12}$-sup models with the adsorbed reactants and products. It turns out that Δ_{sup} is 0.8 just for one of the cases in Table 1 indicating that the differences in reaction energy between the $Mo_{12}C_{12}$-free and $Mo_{12}C_{12}$-sup models cannot always be fully attributed to structural changes, which implies that a full description of the energy profiles, including the reaction energy value, requires taking the Au support into account. Besides, for the other two cases studied, Δ_{sup} becomes 2.1 and −0.7. The large deviation from 1 meaning that the difference in reaction energy is not driven by the structural changes in the NP, instead they are induced by the support. Nevertheless, the positive part of this comparison is that $Mo_{12}C_{12}$-free and $Mo_{12}C_{12}$-sup provide a very similar description of the CO_2 adsorption and energy barrier, considering the bottleneck parameters on CO_2 activation, which justifies the use of the $Mo_{12}C_{12}$-free model to explore the reactivity of the H-covered NPs. It is also worth pointing out that the partially relaxed $Mo_{12}C_{12}$-free-1 and $Mo_{12}C_{12}$-free-2 models do not adequately represent the situation for the supported particle as, in the absence of a support, a minimal reconstruction is required to recover the capability of the $Mo_{12}C_{12}$ NP to adsorb and activate CO_2.

Next, we make use of the $Mo_{12}C_{12}$-free models to systematically explore additional reaction pathways always with the same conclusion, the CO_2 direct dissociation is not favored which, again, is in line with experimental findings where no methane is detected, and CO and methanol are the only products, see Figure 3. Since CO_2 dissociation is experimentally observed when a significant amount of hydrogen is present (cf., Figures 3 and 4), a new series of calculations were carried out to explore the effect of coadsorbed atomic H on the CO_2 dissociation energy profile. For the situations where one H atom is present close to the adsorbed CO_2 molecule, the energy barrier for dissociation is still large, above 0.4 eV, essentially as when H is not present.

This is clear when comparing the direct dissociation through the named path 3 with an almost equivalent activation pathway for a low hydrogen regime, hereafter referred to as path 3H. This pathway involves two steps, the first one corresponds to the dissociation of adsorbed CO_2, which is equivalent to the process observed when hydrogen is not present, and the second step involves hydrogenation of adsorbed O, as schematically shown in Figure 6 top. Consequently, the formation of a carboxylate (COOH) adsorbed species, a key species in the reverse water−gas shift mechanism,[14] is circumvented. The same situation is encountered when analyzing other pathways involving different sites. Most explored hydrogenation steps either failed to converge to the carboxylate intermediate leading instead to adsorbed CO and OH directly, or involved exceedingly large energy barriers. In any case, path 3 and path 3H allow a meaningful comparison between direct and hydrogen-assisted CO_2 activation as both mechanisms involve similar elementary steps with nearly equal energy barriers, 0.38 and 0.44 eV for path 3 and path 3H, respectively. These energy barriers are sufficiently high to prevent easy dissociation which agrees with the experimental findings that, in the absence of a sufficient amount of hydrogen, these Mo_2C NPs are not active for CO_2 dissociation.

Therefore, we analyzed the situation involving a high hydrogen regime already studied with experiment and theory in a previous work showing that the interaction between hydrogen and the MoC NPs supported on Au(111) occurs either *via* adsorption on top of C atoms in a *Kubas* mode as well as on top-Mo.[9] The model calculations carried out for the interaction of CO_2 with the $Mo_{12}C_{12}$-free NPs covered with more H atoms reveal a systematic lowering of the energy barrier for CO_2 dissociation. In particular, the formation of a *Kubas* complex—an elongated H_2 moiety—has an important impact on the energy barrier for CO_2 dissociation which becomes significantly reduced with values as low as 0.2−0.3 eV, and always involving the direct formation of CO and OH, again with no evidence of stable adsorbed COOH, at least at a

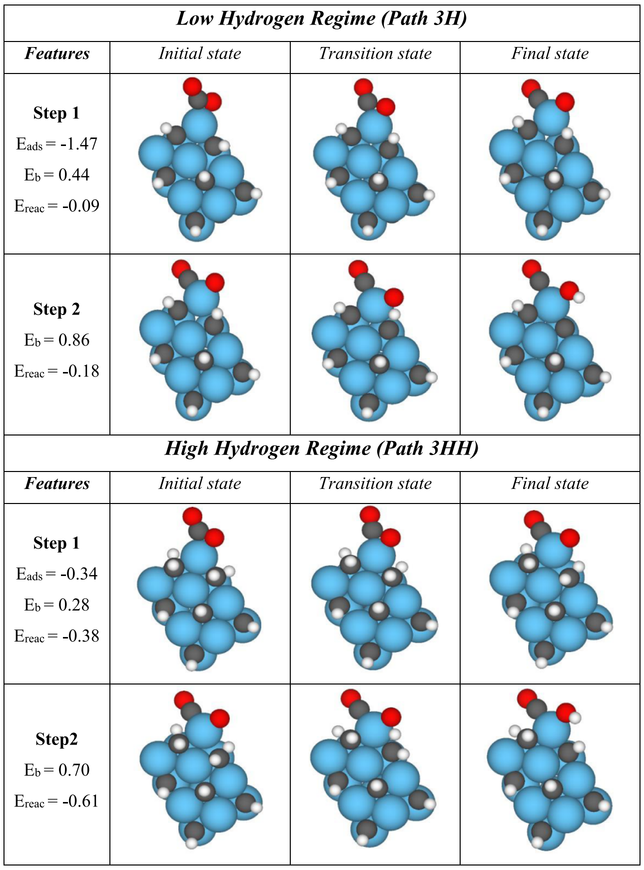

Figure 6. CO_2 hydrogenation paths on different hydrogen regimes for the $Mo_{12}C_{12}$-free model. Top and bottom panels correspond to the low and high H regime situations, respectively. Blue, black, red, and white spheres correspond to Mo, C, O, and H atoms, respectively. Values listed in the left side are as in Figure 5. All energies are given in eV.

competitive level. The differences with respect to the cases with no adsorbed H or with low H coverage are small but significative. Moreover, the computational setup explained in the previous section allows us to rule out the possibility of a numerical artifact. Nevertheless, to directly examine the influence of a high hydrogen regime in an analogous situation to the already mentioned example, we consider again path 3 but in a high hydrogen regime (path 3 HH). For this situation, the relevant results are reported in Figure 6 bottom. For path 3 HH, the molecular mechanism is in the low hydrogen regime path 3 H but with a significant drop in the energy barrier for CO_2 direct dissociation from 0.44 to 0.28 eV. This is an additional clear indication of the important effect of H coverage on the mechanism for CO_2 conversion.

To complete the study and to better model the experimental situation where the partial pressure ratio for CO_2 and H_2 gases is 19, a full H coverage model has been investigated where 19 H atoms are incorporated to the $Mo_{12}C_{12}$-free, where gas-phase CO_2 reacts with the adsorbed H atoms to form a formate intermediate following an Eley–Rideal mechanism. Interestingly, the energy barrier for such an elementary step is significantly small, of only 0.2 eV, and smaller than those corresponding to direct CO_2 dissociation in the absence of adsorbed H, see Figure 7. In conclusion, in spite of inherent limitations of the models used to represent the C-rich MoC_x/Au(111) system, the present DFT calculations consistently predict that the presence of a significant amount of adsorbed atomic H significantly lowers the energy barrier for CO_2 dissociation leading to CO either *via* direct dissociation or through a formate intermediate, the latter implying an Eley–Rideal mechanism. Therefore, the predictions from the present model calculations are in qualitative agreement with experimental findings and provide consistent insights into the involved molecular mechanism evidencing the important effect of preadsorbed H on the CO_2 conversion to CO, although the calculated energy barriers should not be taken as estimates of the experimental values. In particular, the mentioned Eley–Rideal mechanism is likely to explain the formation of methanol as this requires continued hydrogenation steps to the adsorbed formate intermediate.

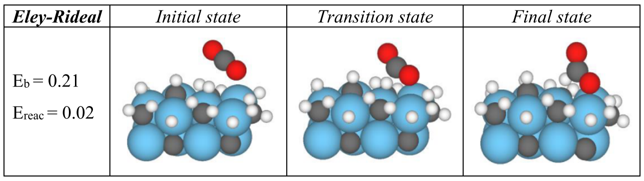

Figure 7. Eley–Rideal mechanism for CO_2 hydrogenation on a H-covered $Mo_{12}C_{12}$-free. Note that the bottom layer does not contain H because it is the region that should be in contact with the Au support. Color code as in Figure 6. All energies are given in eV.

■ CONCLUSIONS

Carbon-poor ($MoC_{0.6}$) and carbon-rich ($MoC_{1.1}$) carbide NPs supported on Au(111) are active for the hydrogenation of CO_2. The molecule underwent partial ($CO_2 \rightarrow CO + O$) and complete ($CO_2 \rightarrow C + 2O$) decomposition on the $MoC_{0.6}$/Au(111) surface. This system was highly active but unstable under CO_2 hydrogenation conditions, producing CO and methane as main products with a very minor amount of methanol. In contrast, the nearly stoichiometric NPs in $MoC_{1.1}$/Au(111) reversibly adsorbed/desorbed CO_2 and, after exposure to hydrogen, CO_2 was converted predominantly to CO with a significant amount of methanol and no methane or other alkanes as reaction products. The apparent activation energy for this process (14 kcal/mol) was smaller than that corresponding to bulk δ-MoC (17 kcal/mol) or a Cu(111) benchmark system (25 kcal/mol). This trend reflects the superior ability of $MoC_{1.1}$/Au(111) to bind and dissociate H_2.

DFT calculations carried out for free or supported $Mo_{12}C_{12}$ NPs showed that, in the absence of preadsorbed H, the direct dissociation involves rather large energy barriers, which is in agreement with the experiment. The fact that calculations for the Au-supported and free $Mo_{12}C_{12}$ NP models lead to the same qualitative description of the reaction mechanism, with almost quantitative agreement for the adsorption energy and energy barrier for CO_2 dissociation, opens the way to the use of the unsupported model to investigate the catalytic properties of these NPs. These show that the large reservoir of H adatoms present in a $Mo_{12}C_{12}$ NP led to a considerable reduction in the energy barrier for the CO_2 dissociation to CO and OH without evidence of a carboxylate intermediate, thus providing a detailed insight into the experimental observations. Nevertheless, we must point out that the energy barriers predicted with the present models featuring different hydrogen coverages have to be taken as an indication of the overall effect and should not be directly compared to experimentally derived values. For the high H coverage situation, the present model calculations suggest that the pathway to methanol is likely to involve an Eley−Rideal mechanism leading to a formate intermediate that, we speculate, undergoes a series of hydrogenation steps.

■ ASSOCIATED CONTENT

Supporting Information

The Supporting Information is available free of charge at https://pubs.acs.org/doi/10.1021/acscatal.1c01738.

Atomic coordinates for representative models (PDF)

■ AUTHOR INFORMATION

Corresponding Authors

José A. Rodriguez − *Chemistry Division, Brookhaven National Laboratory, Upton, New York 11973, United States;* orcid.org/0000-0002-5680-4214; Email: rodrigez@bnl.gov

Francesc Illas − *Departament de Ciència de Materials i Química Física & Institut de Química Teòrica i Computacional (IQTCUB), Universitat de Barcelona, 08028 Barcelona, Spain;* orcid.org/0000-0003-2104-6123; Email: francesc.illas@ub.edu

Authors

Marc Figueras − *Departament de Ciència de Materials i Química Física & Institut de Química Teòrica i Computacional (IQTCUB), Universitat de Barcelona, 08028 Barcelona, Spain*

Ramón A. Gutiérrez − *Facultad de Ciencias, Universidad Central de Venezuela, 1020-A Caracas, Venezuela; Chemistry Division, Brookhaven National Laboratory, Upton, New York 11973, United States*

Francesc Viñes − *Departament de Ciència de Materials i Química Física & Institut de Química Teòrica i Computacional (IQTCUB), Universitat de Barcelona, 08028 Barcelona, Spain;* orcid.org/0000-0001-9987-8654

Pedro J. Ramírez − *Facultad de Ciencias, Universidad Central de Venezuela, 1020-A Caracas, Venezuela;* Present Address: Zoneca-CENEX, R&D Laboratories, Alta Vista, 64770 Monterrey, Mexico

Complete contact information is available at: https://pubs.acs.org/10.1021/acscatal.1c01738

Notes

The authors declare no competing financial interest.

■ ACKNOWLEDGMENTS

The research carried out at the Universitat de Barcelona has been supported by the Spanish MICIUN/FEDER RTI2018-095460-B-I00 and María de Maeztu MDM-2017-0767 grants and, in part, by Generalitat de Catalunya 2017SGR13 grants. This manuscript has been authored by employees of Brookhaven Science Associates, LLC under contract no. DE-SC0012704 with the U.S. Department of Energy. F.I. acknowledges additional support from the 2015 ICREA Academia Award for Excellence in University Research. Computational resources provided by the Red Española de Supercomputación are fully acknowledged.

■ REFERENCES

(1) Levy, R. B.; Boudart, M. Platinum-Like Behavior of Tungsten Carbide in Surface Catalysis. *Science* **1973**, *181*, 547−549.

(2) Hwu, H. H.; Chen, J. G. Surface Chemistry of Transition Metal Carbides. *Chem. Rev.* **2005**, *105*, 185−212.

(3) Shou, H.; Davis, R. J. Multi-Product Steady-State Isotopic Transient Kinetic Analysis of CO Hydrogenation over Supported Molybdenum Carbide. *J. Catal.* **2013**, *306*, 91−99.

(4) Silveri, F.; Quesne, M. G.; Roldán, A.; de Leeuw, N. H.; Catlow, C. R. A. Hydrogen Adsorption on Transition Metal Carbides: a DFT Study. *Phys. Chem. Chem. Phys.* **2019**, *21*, 5335−5343.

(5) Vo, D.-V. N.; Adesina, A. A. Fischer-Tropsch Synthesis over Alumina-Supported Molybdenum Carbide Catalyst. *Appl. Catal., A* **2011**, *399*, 221−232.

(6) Gao, J.; Zheng, Y.; Fitzgerald, G. B.; de Joannis, J.; Tang, Y.; Wachs, I. E.; Podkolzin, S. G. Structure of Mo_2C_x and Mo_4C_x Molybdenum Carbide Nanoparticles and Their Anchoring Sites on ZSM-5 Zeolites. *J. Phys. Chem. C* **2014**, *118*, 4670−4679.

(7) Prats, H.; Piñero, J. J.; Viñes, F.; Bromley, S. T.; Sayós, R.; Illas, F. Assessing the Usefulness of Transition Metal Carbides for Hydrogenation Reactions. *Chem. Commun.* **2019**, *55*, 12797−12800.

(8) Figueras, M.; Gutiérrez, R. A.; Prats, H.; Viñes, F.; Ramírez, P. J.; Illas, F.; Rodriguez, J. A. Boosting the Activity of Transition Metal Carbides Towards Methane Activation by Nanostructuring. *Phys. Chem. Chem. Phys.* **2020**, *22*, 7110−7118.

(9) Figueras, M.; Gutiérrez, R. A.; Viñes, F.; Ramírez, P. J.; Rodriguez, J. A.; Illas, F.; Rodriguez, J. A. Supported Molybdenum Carbide Nanoparticles as Hot Hydrogen Reservoirs for Catalytic Applications. *J. Phys. Chem. Lett.* **2020**, *11*, 8437−8441.

(10) Anderson, T. R.; Hawkins, E.; Jones, P. D. CO_2, the greenhouse effect and global warming: from the pioneering work of Arrhenius and Callendar to today's Earth System Models. *Endeavour* **2016**, *40*, 178−187.

(11) Porosoff, M. D.; Yan, B.; Chen, J. G. Catalytic reduction of CO_2 by H_2 for synthesis of CO, methanol and hydrocarbons: challenges and opportunities. *Energy Environ. Sci.* **2016**, *9*, 62−73.

(12) Aresta, M. *Carbon Dioxide as Chemical Feedstock*; Wiley-VCH: New York, 2010.

(13) Baddour, F. G.; Roberts, E. J.; To, A. T.; Wang, L.; Habas, S. E.; Ruddy, D. A.; Bedford, N. M.; Wright, J.; Nash, C. P.; Schaidle, J. A.; Brutchey, R. L.; Malmstadt, N. An Exceptionally Mild and Scalable Solution-Phase Synthesis of Molybdenum Carbide Nanoparticles for Thermocatalytic CO_2 Hydrogenation. *J. Am. Chem. Soc.* **2020**, *142*, 1010−1019.

(14) Posada-Pérez, S.; Ramírez, P. J.; Evans, J.; Viñes, F.; Liu, P.; Illas, F.; Rodriguez, J. A. Highly Active Au/δ-MoC and Cu/δ-MoC Catalysts for the Conversion of CO_2: The Metal/C Ratio as a Key Factor Defining Activity, Selectivity, and Stability. *J. Am. Chem. Soc.* **2016**, *138*, 8269−8278.

(15) Posada-Pérez, S.; Viñes, F.; Ramirez, P. J.; Vidal, A. B.; Rodriguez, J. A.; Illas, F. The Bending Machine: CO_2 Activation and Hydrogenation on δ-MoC(001) and β-Mo_2C(001) Surfaces. *Phys. Chem. Chem. Phys.* **2014**, *16*, 14912−14921.

(16) Xu, W.; Ramirez, P. J.; Stacchiola, D.; Rodriguez, J. A. Synthesis of α-MoC_{1-x} and β-MoC_y Catalysts for CO_2 Hydrogenation by Thermal Carburization of Mo-oxide in Hydrocarbon and Hydrogen Mixtures. *Catal. Lett.* **2014**, *144*, 1418−1424.

(17) Kunkel, C.; Viñes, F.; Illas, F. Transition Metal Carbides as Novel Materials for CO_2 Capture, Storage, and Activation. *Energy Environ. Sci.* **2016**, *9*, 141−144.

(18) Horn, J. M.; Song, Z.; Potapenko, D. V.; Hrbek, J.; White, M. G. Characterization of Molybdenum Carbide Nanoparticles Formed on Au(111) Using Reactive-Layer Assisted Deposition. *J. Phys. Chem. B* **2005**, *109*, 44−47.

(19) Rodriguez, J. A.; Liu, P.; Dvorak, J.; Jirsak, T.; Gomes, J.; Takahashi, Y.; Nakamura, K. The interaction of oxygen with TiC(001): Photoemission and first-principles studies. *J. Chem. Phys.* **2004**, *121*, 465−474.

(20) Frantz, P.; Didziulis, S. V. Detailed spectroscopic studies of oxygen on metal carbide surfaces. *Surf. Sci.* **1998**, *412*−*413*, 384.

(21) Didziulis, S. V.; Frantz, P.; Perry, S. S.; El-bjeirami, O.; Imaduddin, S.; Merrill, P. B. Substrate-Dependent Reactivity of Water on Metal Carbide Surfaces. *J. Phys. Chem. B* **1999**, *103*, 11129.

(22) Potapenko, D.; Horn, J.; White, M. The Reactions of Cyclohexene on Au(111)-supported Molybdenum Carbide Nanoparticles. *J. Catal.* **2005**, *236*, 346−355.

(23) Lamiel-Garcia, O.; Bromley, S. T.; Illas, F. Low-energy Nanoscale Clusters of $(TiC)_n$ n = 6, 12: A Structural and Energetic Comparison with MgO. *Theor. Chem. Acc.* **2013**, *132*, 1312−1318.

(24) Jiménez-Orozco, C.; Figueras, M.; Flórez, E.; Viñes, F.; Rodriguez, J. A.; Illas, F. Size and Stoichiometry Effects on the Reactivity of MoC_y Nanoparticles Towards Ethylene. *J. Phys. Chem. C* **2021**, *125*, 6287−6297.

(25) Lozano-Reis, P.; Prats, H.; Gamallo, P.; Illas, F.; Sayós, R. Multiscale Study of the Mechanism of Catalytic CO_2 Hydrogenation: Role of the Ni(111) Facets. *ACS Catal.* **2020**, *10*, 8077−8089.

(26) Piqué, O.; Viñes, F.; Illas, F.; Calle-Vallejo, F. Elucidating the structure of ethanol-producing active sites at oxide-derived Cu electrocatalysts. *ACS Catal.* **2020**, *10*, 10488−10494.

(27) Chen, B. W. J.; Xu, L.; Mavrikakis, M. Computational Methods in Heterogeneous Catalysis. *Chem. Rev.* **2021**, *121*, 1007−1048.

(28) Morales-García, A.; Viñes, F.; Gomes, J. R. B.; Illas, F. Concepts, models and methods in computational heterogeneous catalysis illustrated through CO_2 conversion. *Wiley Interdiscip. Rev.: Comput. Mol. Sci.* **2021**, *11*, No. e1530.

(29) Kresse, G.; Furthmüller, J. Efficient Iterative Schemes for ab initio Total-energy Calculations Using a Plane-wave Basis Set. *Phys. Rev. B: Condens. Matter Mater. Phys.* **1996**, *54*, 11169−11186.

(30) Perdew, J. P.; Burke, K.; Ernzerhof, M. Generalized Gradient Approximation Made Simple. *Phys. Rev. Lett.* **1996**, *77*, 3865−3868.

(31) Politi, J. R. D. S.; Viñes, F.; Rodriguez, J. A.; Illas, F. Atomic and Electronic Structure of Molybdenum Carbide Phases: Bulk and Low Miller-index Surfaces. *Phys. Chem. Chem. Phys.* **2013**, *15*, 12617−12625.

(32) Grimme, S.; Antony, J.; Ehrlich, S.; Krieg, H. A consistent and accurate ab initio parametrization of density functional dispersion correction (DFT-D) for the 94 elements H-Pu. *J. Chem. Phys.* **2010**, *132*, 154104.

(33) Kresse, G.; Joubert, D. From ultrasoft pseudopotentials to the projector augmented-wave method. *Phys. Rev. B: Condens. Matter Mater. Phys.* **1999**, *59*, 1758−1775.

(34) Henkelman, G.; Uberuaga, B. P.; Jónsson, H. A Climbing Image Nudged Elastic Band Method for Finding Saddle Points and Minimum Energy Paths. *Phys. Rev. B: Condens. Matter Mater. Phys.* **2000**, *113*, 9901−9904.

(35) Posada-Pérez, S.; Ramírez, P. J.; Gutiérrez, R. A.; Stacchiola, D. J.; Viñes, F.; Liu, P.; Illas, F.; Rodriguez, J. A. The Conversion of CO_2 to Methanol on orthorhombic β-Mo_2C and Cu/β-Mo_2C Catalysts: Mechanism for Admetal Induced Change in the Selectivity and Activity. *Catal. Sci. Technol.* **2016**, *6*, 6766−6777.

(36) Likith, S. R. J.; Farberow, C. A.; Manna, S.; Abdulslam, A.; Stevanović, V.; Ruddy, D. A.; Schaidle, J. A.; Robichaud, D. J.; Ciobanu, C. V. Thermodynamic Stability of Molybdenum Oxycarbides Formed from Orthorhombic Mo_2C in Oxygen-Rich Environments. *J. Phys. Chem. C* **2018**, *122*, 1223−1233.

(37) Kurlov, A.; Huang, X.; Deeva, E. B.; Abdala, P. M.; Fedorov, A.; Müller, C. R. Molybdenum carbide and oxycarbide from carbon-supported MoO_3 nanosheets: phase evolution and DRM catalytic activity assessed by TEM and in situ XANES/XRD methods. *Nanoscale* **2020**, *12*, 13086.

(38) Yoshihara, Y.; Campbell, H. Methanol Synthesis and Reverse Water-Gas Shift Kinetics over Cu(110) Model Catalysts: Structural Sensitivity. *J. Catal.* **1996**, *161*, 776−782.

(39) Schumann, J.; Tarasov, A.; Thomas, N.; Schlögl, R.; Behrens, M. Cu,Zn-based catalysts for methanol synthesis: On the effect of calcination conditions and the part of residual carbonates. *Appl. Catal., A* **2016**, *516*, 117.

(40) Figueras, M.; Jurado, A.; Morales-García, Á.; Viñes, F.; Illas, F. Bulk (in)stability as a possible source of surface reconstruction. *Phys. Chem. Chem. Phys.* **2020**, *22*, 19249−19253.